Quantitative analysis of cell motion during sorting in two-dimensional aggregates of dissociated hydra cells

Jean Paul Rieu,* Naoki Kataoka, and Yasuji Sawada
Research Institute of Electrical Communication, Tohoku University, 2-1-1 Katahira, Aoba-ku, Sendai 980-77, Japan
(Received 12 February 1997; revised manuscript received 21 July 1997)

We investigate cell motion during cell sorting in aggregates of dissociated hydra cells. *Hydra viridissima* combined with a two-dimensional experimental geometry allows us to track endodermal cells and to quantify cell and cluster motion statistically. Individual endodermal cells move randomly in the absence of bulk coherent motion. This random motion due to membrane fluctuations contributes to the formation of endodermal clusters. Cell sorting is accomplished by the contact between clusters due to their random deformation, and by the rounding of coalesced clusters. Coherent motion contributes to rounding both of the endodermal clusters and the aggregate. [S1063-651X(97)07312-1]

PACS number(s): 87.45.Bp, 87.22.−q, 05.60.+w

I. INTRODUCTION

When multiple types of cells from a primitive animal or an embryo are dissociated, randomly intermingled, and then reaggregated, they are able to rearrange, to reestablish coherent homotypic domains, and sometimes to reconstitute an entire animal. This rearrangement of cells, known as cell sorting, offers insight into the mechanisms governing morphogenesis and wound healing. Sorting has long been studied using organisms including hydra [1]. Hydra have a strong regenerative capacity [2–4]. From a mixture of dissociated endodermal and ectodermal epithelial cells, an external monolayer of ectodermal cells forms in a few hours, then the aggregate develops an internal cavity within 20 h, and within one week a normal hydra regenerates [2,3]. Technau and Holstein observed the number of ectodermal cells appearing on the surface of dissociated cell aggregates [5]. Sorting of neural retinal and pigmented retinal chicken embryo cells has been more intensively investigated [6–9]. Within two or three days, complete sorting occurs: the pigmented cells form a single rounded mass surrounded by neural cells.

Steinberg proposed that cell sorting is driven by surface energy minimization [8,10]. The differential adhesion hypothesis (DAH) postulates that tissues possess interfacial tensions arising from the adhesive interactions between individual cells, and predicts that mixed populations of sufficiently mobile cells rearrange so that the less cohesive cells envelop the more cohesive cells. The surface tensions of different chicken embryonic tissues have been measured using a parallel plate compression apparatus [11]. The relative magnitudes of these tensions predict correctly the mutual envelopment of these tissues. The adhesive forces between pairs of hydra cells have also been estimated using laser tweezers [12]. Endodermal cells are more cohesive than ectodermal cells, as assumed by the DAH. Using a Potts model and the DAH, Glazier and Graner [13] simulated various biological phenomena, including cell sorting.

The DAH explains many macroscopic observations without microscopic assumptions about cell adhesion or cell dynamics. A realistic picture of cell adhesion has to take into account the energy dissipation arising from the formation and separation of adhesive contacts, and the reversible free-energy potential [14,15]. Cell motion may be random [6,7,16], directed due to chemotaxis [17], or coherent by some other mechanism [18–20]. Simulations have shown that random motion is sufficient for cell sorting [13], but very few quantitative results from experimental observations are available. Recently, Mombach and Glazier showed that chicken embryo pigmented cells move randomly in very dilute aggregates (one pigmented cell to 10^4 neural cells), but did not study equal cell mixtures [16].

We report quantitative results for cell sorting dynamics in two dimensional (2D) aggregates of mixed ectodermal and endodermal hydra cells in various proportions. We try to quantify what part of cell motion is random, how random it is and the origin of any coherent motion.

II. MATERIALS AND METHODS

Strain and culture. Hydra viridissima shows good contrast between unstained endodermal and ectodermal cells due to the presence of symbiotic algae inside endodermal cells [21]. Hydra supplied by Dr. H. Shimizu (National Institute of Genetics, Mishima, Japan) were cultured at 18 °C in Loomis' solution [2], fed four times a week with freshly hatched *Artemia nauplii* shrimp, and transfered to a fresh culture solution five hours after feeding. The animals were starved for 24–36 h before experiments.

Preparation of dissociated cell aggregates. Mechanical dissociation and reaggregation of hydra cells were carried out in a dissociation medium (DM) at 4 °C according to the method of Gierer *et al.* [2]. After heads and feet were removed from a group of 3–5 animals, the body columns were minced and almost completely dissociated into single cells by gentle shearing by repeated pipetting. The cell preparation (5–8 ml) was kept 30 min in a DM at 4 °C to sediment and sheared again. It was then filtered using a 53-μm nylon mesh (NRK, Tokyo, Japan) and centrifuged at 250 g for 5 min to sediment and collect the epithelial cells. The upper half of the preparation, consisting of a turbid solution of predominantly interstitial cells was removed, and the remaining cell

*Present address: CEA/Grenoble/DRFMC/SI3M, 17 rue des Martyrs, 38054 Grenoble Cedex 9, France.

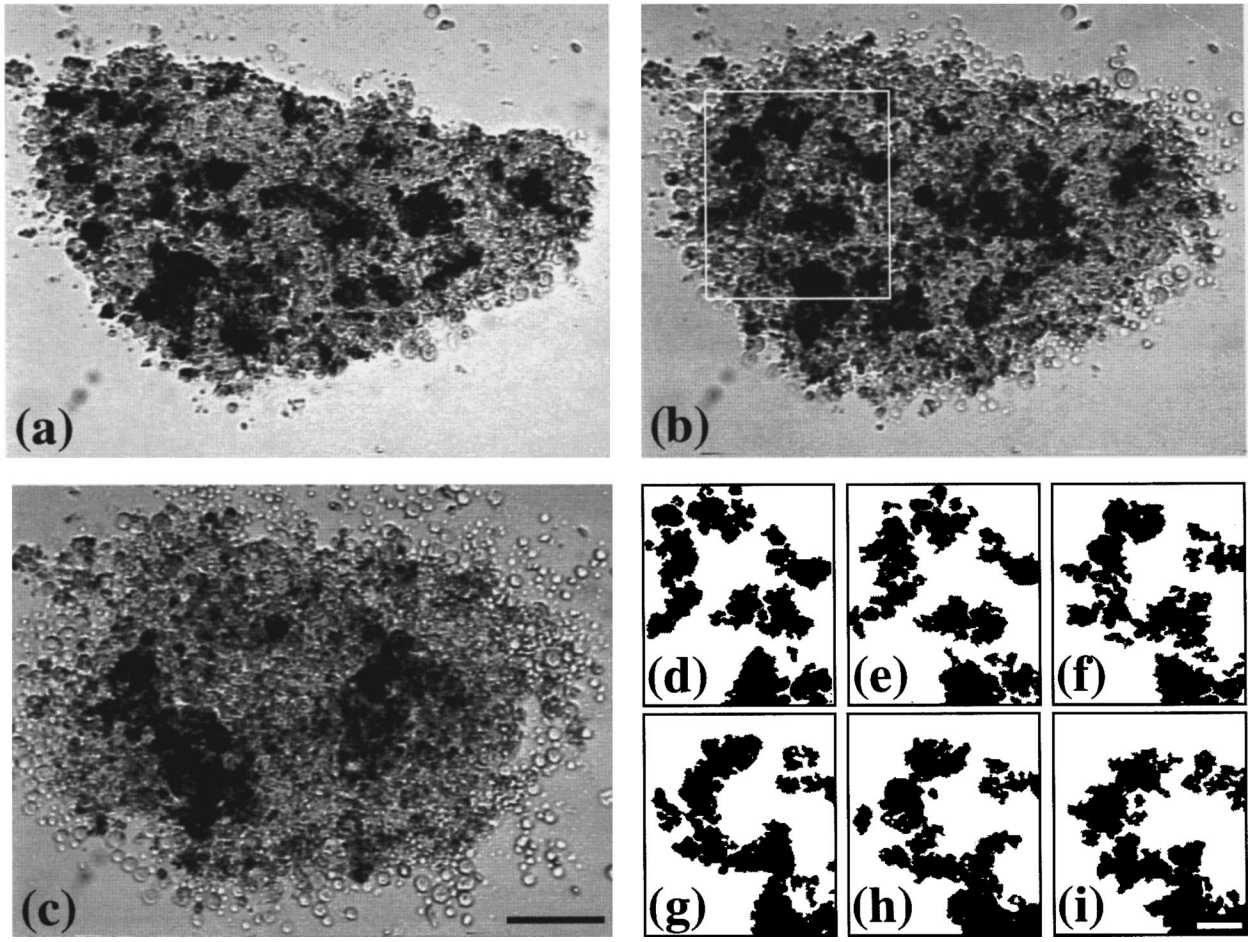

FIG. 1. Sample 1 cell sorting: aggregate with 900 cells [40% endodermal (dark) and 60% ectodernal cells (light)]. (a) Starting configuration showing both endodermal clusters of several cells and single endodermal cells. (b) 1 h; clusters merge together, and aggregate slowly. (c) 4 h; two large clusters are surrounded by ectoderm with some isolated endodermal cells (dark spots). (d)–(i) binary images at 15-min time intervals [from 40 min (d)] from the upper left of the aggregate [frame drawn in (b)]. Bar: 100 μm [(a)–(c)] and 50 μm [(d)–(i)].

pellet was resuspended in a 1-ml DM by gentle pipetting. The cell preparation was once more centrifuged 5 min at 150 g in two 0.5-ml conical tubes to form the final aggregate of dissociated cells. For experiments with a given ratio of one cell type, instead of dissociating whole tissue and making aggregates of mixed cells, the ectodermal and endodermal layers were separated using procaine-HCl (Wako Pure Chemicals, Tokyo, Japan) according to the method of Ref. [22]. Aggregates were then prepared as described previously with a given number of each cell type.

The 2D experimental setup. The sample was put on glass slide between a pair of 25-μm spacers and then gently covered with another slide. Slides were fixed together with clips and transfered to a Petri dish containing a DM solution at 18 °C. The dish was placed on an inverted microscope (Olympus, Japan) and observed with a color charge-coupled device camera. Experiments were recorded by a time-lapse videotape recorder (Sony CVD-1000, Japan) at an interval of 15 or 30 s per frame. Later, at intervals of $5-20$ min, images were digitized and analyzed on a computer using a NIH image [23]. The positions of single cells were manually marked, the centers of mass of clusters of a few cells were calculated with NIH and their trajectories reconstructed.

2D aggregate survival. Experiments were analyzed until the first signs of sample disaggregation (4–16 h). At that time, cell density significantly decreased, cell mobility almost stopped, and endodermal clusters became less cohesive and slowly disaggregated. Later, cells died. We investigated two special kinds of slide: glass covered with human albumin (Wako Pure Chemicals, Tokyo), and porous glass (Giken Science Co., Japan). Albumin reduces the cell-substrate adhesion [24], and thus might increase cell mobility and accelerate sorting. Porous glass might prevent cell density decrease due to a lack of oxygen. However, the sorting time was independent of the glass used.

Analysis of aggregates and cells. We analyzed the movements of single cells and clusters of a few cells in four mixed aggregates, with endodermal cell concentrations ranging from 55% to 17%. Additional experiments in mixed aggregates, in particular those with an endodermal concentration higher than 60%, were not analyzed because the endodermal cells quickly percolated, making it impossible to identify individual cells or clusters. Unless noted, we refer to endodermal cells. For single endodermal cells, we distinguish *nonaggregating cells* from *aggregating cells*. *Nonaggregating cells* move inside the continuous mass of ectodermal cells without attaching to any cluster during the experiment.

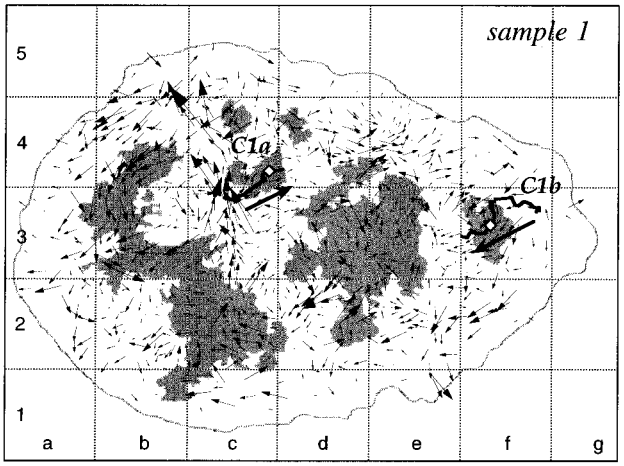

FIG. 2. Cell displacements of 850 cells (both endodermal and ectodermal) during the time interval 120–150 min, in sample 1. The arrow size is proportional to the cell displacement. The gray background represents the cluster configuration at 2 h. The positions of the two clusters labeled $C1a$ (ten cells) and $C1b$ (eight cells) are marked with a white diamond, and their trajectories between 0 and 3 h 30 min and directions are displayed with thick lines and arrows. Box size, 100 μm.

III. EXPERIMENTAL OBSERVATIONS

A. Aggregates with similar proportions of both cell types

The sequence of events in an aggregate with 40% endodermal cells (dark) is displayed in Fig. 1 (sample 1). At the beginning of the experiment [Fig. 1(a)], the population of endodermal cells consists both of single cells and clusters of several cells which are surrounded by a continuous mass of ectodermal cells (light). During the first few hours, as the aggregate slowly rounds, internal clusters grow by fusing with one another and with single cells [Fig. 1(b)]. Sorting is nearly complete after 4 h: two compact endodermal islands are surrounded by ectodermal cells [Fig. 1(c)]. At this time, many dead cells appear at the periphery of the aggregate (they can be distinguished from living cells by their larger size and circular shape). Later, the sample slowly disaggregates. The experimental lifetime is longer in larger aggregates, but as the cells are initially more distant, we never obtained a final configuration with only one endodermal mass.

Cluster coalescence is shown in binary images of the upper left part of the aggregate [Figs. 1(d)–1(i)]. At 40 min [Fig. 1(d)], endodermal cells form 3–5 cell clusters. These small clusters undergo randomly oriented changes in shape apparently due to changes in cell position within the clusters. Small amplitude cluster displacements also occur. Cluster deformations bring adjacent clusters into contact [Figs. 1(e)–1(g)]. Once almost all the small clusters have aggregated [Fig. 1(g)], the newly formed large cluster begins to round, though random deformation is still present [Figs. 1(h)–1(i)]. Some isolated clusters behave differently; e.g., C1a and C1b, whose trajectories reconstructed during 3 h 30 min are displayed in Fig. 2. C1a escapes from the aggregating central region in a linear trajectory for 2 h 30 min, then almost stops. C1b has a slightly curved trajectory directed toward the aggregate center. It finally merges with the large endodermal mass nearby.

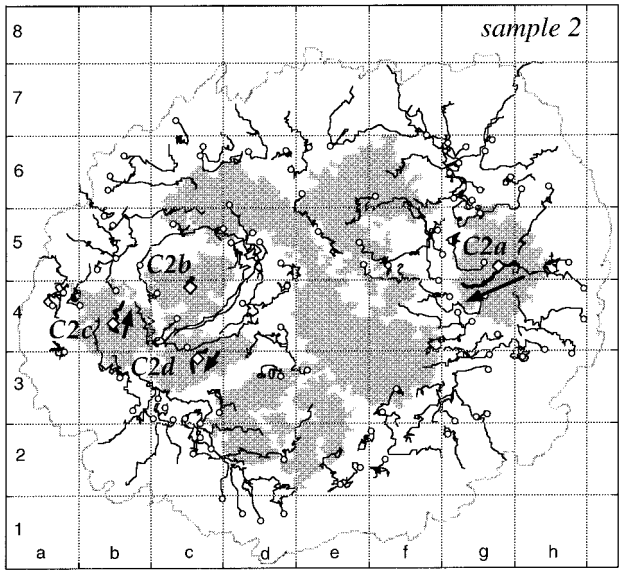

FIG. 3. Trajectory of 100 single endodermal cells during sample 2 cell sorting (aggregate with 2000 cells, 55% endodermal cells). Dots correspond to the initial cell positions. Positions are reported at intervals of 10 min between 0 and 8 h. The gray background represents the cluster configuration at 3 h. The positions of the clusters labeled $C2a$, $C2b$, $C2c$, and $C2d$ (60, 35, 40, and 40 cells, respectively) are marked with a white diamond; their trajectories between 1 and 5 h 30 min and their directions are displayed with a white thick line and arrow. Box size, 100 μm.

In Fig. 2, we also show the displacements of 850 cells (both endodermal and ectodermal) between 2 h and 2 h 30 min. Displacements of nearest neighbors are generally correlated: locally, cells move in the same direction as coherent groups. Inside the endodermal clusters, this coherent motion participates in rounding (see boxes $b4$, $c2$). In the ectoderm, in some regions of the sample, cells flow around clusters. The circular flow in boxes $c4$-$c5$-$b5$ seems correlated to the neighboring cluster's rounding. The flow tangent to the external boundary in boxes $f2$-$e2$ seems to participate in aggregate rounding as in sample 4 (see below).

Cluster trajectories and nonaggregating endodermal cell trajectories during sorting in sample 2 are shown in Fig. 3. $C2a$'s trajectory is roughly linear, and directed toward the center of the aggregate. Clusters $C2b$, $C2c$, and $C2d$, once formed, barely move during the whole experiment, though only a few μm away from the main endodermal mass. The other clusters quickly percolate to form the main endodermal island (center). The nonaggregating cell trajectories in Fig. 3 weakly fluctuate over short times (<1 h); however, over long times, they are relatively linear or curved with one or two kinks on average. They seem dependent on the position and motion of neighboring clusters. For instance, endodermal cells in boxes $b6$ or $h4$ tend to occupy the empty space left by clusters moving toward the aggregate center; some cells close to the external boundary are driven by the expansion of the boundary (see boxes $b2$ or $f7$, and $g7$); cells in boxes $c5$, $d5$, and $d4$ flow clockwise circumferentially in a narrow channel between large clusters.

In sample 3, we observed the formation of a 35-cell cluster from initially dispersed single endodermal cells (Fig. 4). This initial stage of cell sorting is not always observed, since

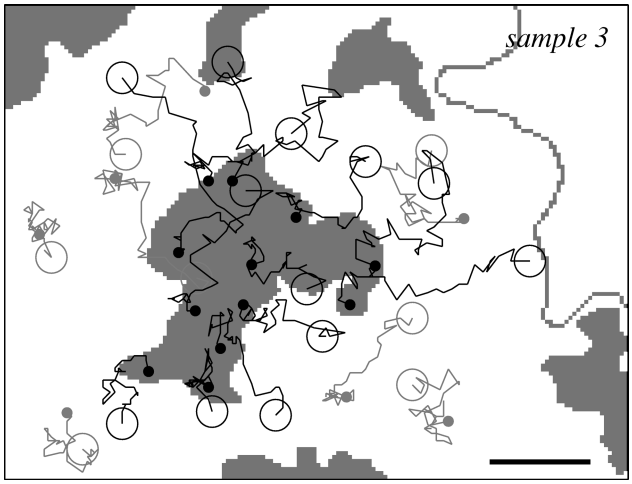

FIG. 4. Cluster formation in sample 3. Aggregating cells (black) and nonaggregating cell (gray) trajectories are reconstructed between 0 and 6 h at intervals of 10 min. Large circles represent the approximate sizes of the cells and their initial positions, bullets give the final position of the cells. The 35-cell cluster contour is represented in the gray background at 6 h. Bar, 50 μm.

we often start with small clusters already present as in sample 1 (Fig. 1). Most of the cell trajectories in Fig. 4 resemble random walks. Some cells initially located more than 50 μm away from their final position in the cluster have directed trajectories, but other cells which are initially closer to the cluster do not aggregate. Thus, it seems that cluster formation is accomplished by random displacements of the aggregating cells.

B. Aggregate with a low endodermal concentration

To observe individual cells, we used aggregates with a low endodermal cell concentration. Figure 5 shows an aggregate, sample 4, with approximatively 17% endodermal cells (dark). At the beginning [Fig. 5(a)], individual endodermal cells and a few endodermal clusters of 2–6 cells are scattered throughout the interior, some at the surface of the aggregate. The initial aggregate shape is elongated. After 4 h [Fig. 5(b)], a large endodermal cluster has formed (at bottom left). Cells and clusters are deeper within the rounded aggregate. Hence, sorting occurs locally but remains partial, as the endodermal cells and clusters are too sparsely distributed to encounter each other.

The endodermal cell trajectories are reconstructed over 5 h in Fig. 5(c). The movements of the peripheral cells on the left and right of the figure are driven by rounding. These cells move in collective pathways along the external boundary in slightly curved trajectories. On the other hand, central cells (in the upper central part of the figure) do not participate in rounding. Their displacements appear randomly oriented. A careful examination of the images at 10-min time intervals in this region of the aggregate shows that cells are able to translocate relative to each other by means of random extensions and contractions of the cell membrane known as pseudopodal or ruffling activity [9,25,26]. The peripheral cells, altough strongly driven by rounding, also exhibit membrane fluctuations and small lateral random displacements. These random fluctuations enable most of the initially dispersed cells at the bottom left of the aggregate to fuse to form the main cluster of Fig. 5(b), as do the aggregating cells of sample 3 (Fig. 4).

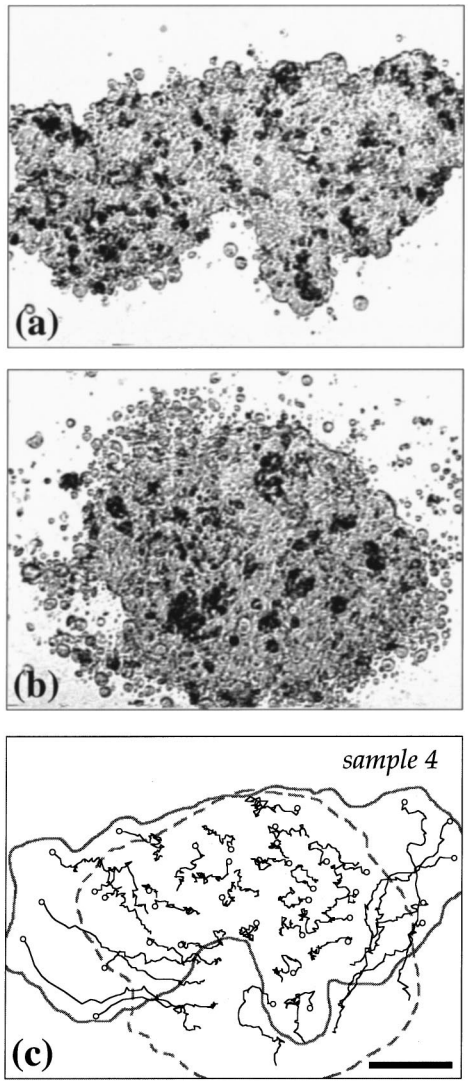

FIG. 5. Sample 4 cell sorting, aggregate with 800 cells (17% endodermal cells). (a) Starting configuration; endodermal cells (mainly single cells) are dispersed throughout the elongated aggregate. (b) 4 h; endodermal cells are more clustered and centered throughout the rounded aggregate. (c) Trajectory of 39 single endodermal cells for 5 h. Dots correspond to the initial cell positions. Positions are reported at intervals of 5 min. Gray thick lines represents the aggregate external boundary at 0 h (solid line) and at 5 h (dotted line). Bar, 100 μm.

IV. QUANTITATIVE ANALYSIS OF SINGLE CELL MOTION

Our main results for single endodermal cells are as follows.

(i) Single cell trajectories have small amplitude random fluctuations over short times. The cells have an autonomous mobility arising from the large ruffling and pseudopodal activity of their cell membranes. In the absence of collective movements [see (ii)], when endodermal cells do not encounter other endodermal cells or clusters, they seem to perform a random walk [aggregating cells in Fig. 4 or central cells in Fig. 5(c)].

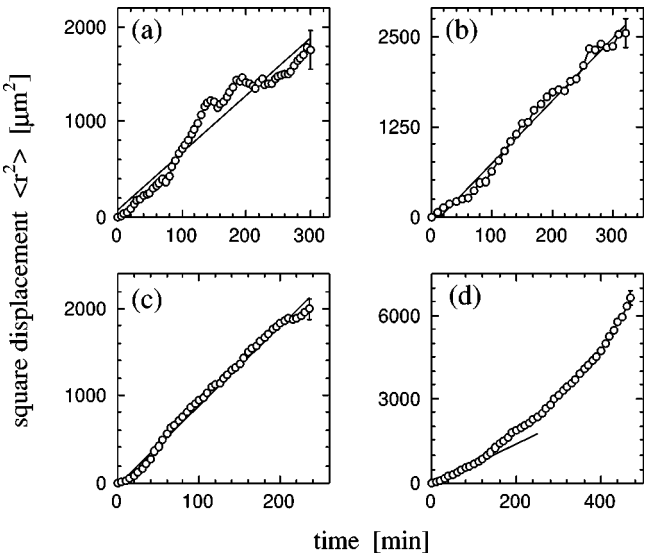

FIG. 6. Average square displacements of single endodermal cells as a function of time for (a) sample 4 (central cells), (b) sample 3, (c) sample 1, and (d) sample 2.

(ii) Over larger times, single cell trajectories are sometimes linear or circular, e.g., when cell displacements are driven by rounding of the aggregate [Fig. 5(c)] or when cell flows appear around rounding and moving clusters (Figs. 2 and 3). Both ectodermal and single endodermal neighboring cell displacements are oriented in the same direction (Fig. 2). We can thus reasonably assume that single endodermal cells, apart from the short time scale random motion, are driven by the continuous flowing mass of ectodermal cells. The nonaggregating endodermal cells then reflect the collective properties of the ectodermal cells.

We next calculate the diffusion constants of single cells and the temporal and spatial correlations of cell velocity. We averaged over all the cells analyzed, obtaining a satisfactory statistics but discarding different behaviors in different parts of the aggregate.

Mean squared displacement. A random walk is described by a diffusion law, $r^2=4Dt$, where D is the 2D diffusion constant, t the time and $\langle r^2\rangle$ is the mean squared displacement. The $\langle r^2\rangle$ of various experiments are shown in Fig. 6. The curves of the central cells of sample 4 [Fig. 6(a)], the aggregating cells of sample 3 [Fig. 6(b)] and the nonaggregating cells of sample 1 [Fig. 6(c)] are approximately linear. Their slopes give similar values for the diffusion constant (1.5, 2.0, and 2.3 μm^2/min, respectively). At long times, $\langle r^2\rangle$ for the nonaggregating cells of sample 2 [Fig. 6(d)] is not linear ($\langle r^2\rangle\sim t^{1.3}$). The behavior is dominated by collective motion of the ectodermal flows. However, these flows arise generally in the narrow channels between newly formed clusters which are not present at early times when the aggregates are still well mixed (see discussion). Thus taking the slope of $\langle r^2\rangle$ over the time interval 0–100 min in Fig. 6(d) yields $D=1.5$ μm^2/min.

Spatial correlations of the velocity. We define the spatial correlations of the velocity by $C(r)=Z(r)/Z(0)$ with $Z(r)=\langle \mathbf{v}(r_i)\cdot\mathbf{v}(r_j)\rangle$ as a function of the distance between cells $r=|r_i-r_j|$. The average is taken over all cells of the same type and over all times analyzed. The correlation for the central cells of sample 4 decreases to zero, and remains

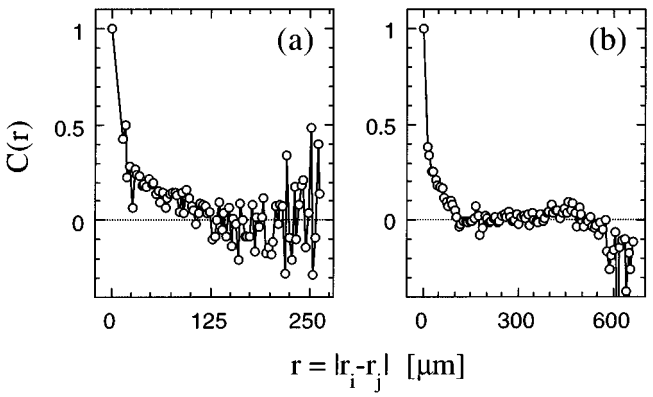

FIG. 7. Average spatial correlation functions of the velocities of single endodermal cells as a function of the distance between pairs of cells for (a) sample 4 (central cells) and (b) sample 2. The average is taken over all pairs of cells during the time interval 0–5 h for (a) and 0–8 h for (b).

zero, indicating uncorrelated velocities at large distances [Fig. 7(a)]. The same behavior occurs for the aggregating cells of Fig. 4. The curve of the nonaggregating cells of sample 2 [Fig. 7(b)] first decreases, then remains around zero, and finally decreases to negative values for large distances ($|r_i-r_j|>500$ μm). We define the correlation length as half of the length, r, at which $C(r)$ vanishes, approximately 50 μm in each experiment. The parallel orientation of displacements of neighboring cells observed in Fig. 2 extends to this distance (i.e., approximatively five cell diameters). The ectodermal flows seen in Fig. 3, oriented in different directions at opposite sides of the aggregate, are responsible for the negative $C(r)$ at large distances in Fig. 7(b).

Temporal correlations of the velocity. The temporal autocorrelation function of the velocity, $C(t)=Z(t)/Z(0)$ with $Z(t)=\langle \mathbf{v}(t_i)\cdot\mathbf{v}(t_j)\rangle$ and $t=|t_i-t_j|$, is reported in Fig. 8 for the same aggregates. The average is over t_i, t_j, and all cells. The autocorrelation function of the *central cells* of *sample 4* [Fig. 8(a)] and of the aggregating cells of sample 3 (not shown) decreases rapidly to zero. At long times, velocities

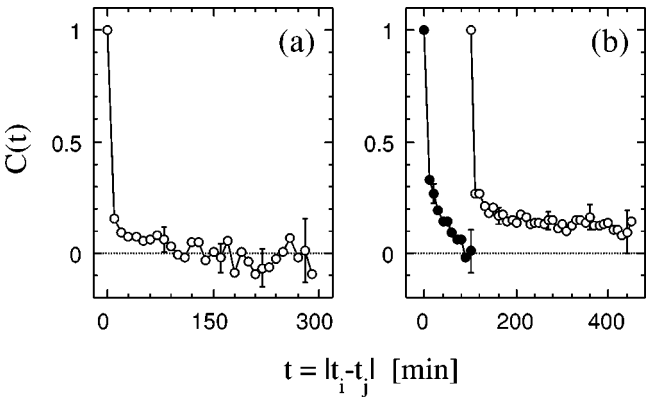

FIG. 8. Average temporal autocorrelation function of the velocity between experimental times t_i and t_j as a function of differential time $t=|t_i-t_j|$ for (a) sample 4 (central cells) and (b) sample 2. The average is taken over all cells and over t_i and t_j within (a) 0–5 h, and (b) 0–100 min (bullets) and 100–480 min (circles). The differential time t was shifted by 100 min for the circles.

are uncorrelated ($C(t)=0$), which is consistent with a random walk. It seems that velocities are slightly correlated over short times ($t<90$ min) but the large error bar due to poor statistics (average over only 25 cells compared with 100 in other experiments) prevents conclusions. Weak correlations may indicate persistence of movement, or that the aggregating cells of Fig. 4 are driven by surface tension for some time after they come into contact.

The temporal correlations of the nonaggregating cells in sample 2 were calculated for early sorting (i.e., t_i and t_j within the experimental time interval 0–100 min, bullets), and for later sorting (100–480 min, circles) [Fig. 8(b)]. In the latter, velocities exhibit very long time correlations as $C(t)$ remains positive up to the end of the experiment. Fitting the data to $a_o\exp(-t/t^*)$, where t^* is the correlation time, we find $t^*=300$ min. In the earlier stage, the correlations are shorter (i.e., $t^*=40$ min) but still much stronger than in Fig. 8(a). A similar correlation time (i.e., $t^*=60$ min) is found for the nonaggregating cells of sample 1.

The collective motions of the endodermal cells analyzed reflect the collective motions of the ectodermal cells. Short range spatial correlations indicate that ectodermal cells move locally as coherent groups. Temporal correlations indicate that these local coherent groups flow in the same direction over some time. In sample 2, once clusters are formed (after 100 min), most of the nonaggregating cells are carried by steady flows of ectodermal cells. At earlier times in this aggregate, or in sample 1, some ectodermal flows exist (see boxes $c3$-$c4$-$b4$ in Fig. 2), but no steady, global circulation. The temporal correlations in sample 2 (before or after 100 min) and sample 1 are consistent with the squared displacement results [Figs. 6(c) and 6(d)]. The displacements of the endodermal cells carried in flows versus time, gives an estimate of the flow velocity, i.e., between 20 and 30 μm/min.

V. DISCUSSION

The single endodermal cell motion analysis shows that cell motion consists of random and correlated parts. During aggregate rounding or sorting, the dynamics of the nonaggregating endodermal cells are dominated by the coherent behavior of the ectodermal cells. In homogeneous aggregates (early sorting or in dilute aggregates), we do not observe long time correlated motion, and the cell behavior is mainly random. The cluster dynamics is similar, though we were not able to perform quantitative measurements.

Random fluctuations of single endodermal cells. Hydra cells have autonomous motility arising from the large ruffling and pseudopodal activity of their cell membranes. In the absence of external biases such as steady coherent motion of the ectodermal cells, isolated endodermal cells perform approximately random walks. The motion differs from a true random walk, since the cells move locally as coherent groups [short range spatial correlations in Fig. 7(a)] with short time-scale correlations [Fig. 8(a)]. The latter may indicate persistent movement as observed during the migration of amoeba and fibroblast cells over surfaces [26]. We are reasonably confident that our estimate of the 2D diffusion constant (i.e., $D=1.5\ \mu m^2/min$) represents the actual rate at which endodermal cells explore randomly their environment, and that it is not biased by coherent motion. First, because this estimate is for cells with quasirandom trajectories and no long time scale correlations, and second because we found a similar value in pure endodermal aggregates once rounding was completed [27]. This value is 45 times larger than the diffusion constant of single pigmented cells in neural cell aggregates made from chicken embryos [16]. The diffusion constant of hydra cells in 3D aggregates has never been evaluated, but should also be larger than in chicken embryos. Chick sorting takes two or three days, while hydra requires 20 h to form a cavity (complex cell rearrangement) [2,3,5]. Thus membrane fluctuations are much more important in hydra cells than in chicken cells, or alternatively the viscosity is higher in chicken aggregates.

Cluster motion. The behavior of endodermal clusters is complex. In the absence of ectodermal flows, they exhibit random deformations and small amplitude random displacements [(Fig. 1(d)–1(i)]. Their cells move randomly within the cluster due to surface tension. As a result, the center of gravity of the cluster moves little, but cluster can deform greatly. The deformations of the neighboring clusters, from time to time, cause their contact. Once firm contact occurs between two clusters, they are pulled to each other by surface tension, leading to aggregation. Similar qualitative observations have been made both in chicken embryo aggregates [7] and in simulations [13]. Though the degree of randomness of cluster deformation or cluster displacements cannot be assessed due to the poor spatial resolution of cluster center of mass and cluster contours, we have studied the movements of a few clusters well isolated from other endodermal cells.

The displacements of the fast moving clusters analyzed ($C1a$, $C1b$, and $C2a$) are roughly linear in time. The values we find for the cluster velocities are 29, 15.9, and 13.0 μm/h, respectively. This quantity is size independent in the experiments presented here and other experiments not shown. Large clusters may move faster or slower than small ones. Generally clusters move toward the center of the aggregate as $C1b$ and $C2a$. However $C1a$ moves toward the periphery with the highest velocity measured in this study. Some clusters are nearly motionless, although very close to the main endodermal mass (the velocities of $C2b$, $C2c$, and $C2d$ are 1.0, 6.4, and 6.1 μm/h, respectively). The fact that cluster motion is not always directed toward the endodermal center of mass indicates that chemotaxis (cells moving along radial concentration gradients within the aggregate) does occur, consistent with the observations of Mombach and Glazier in chicks [16]. The relatively linear trajectories of the fast moving clusters indicate ballistic motion driven by the coherent motion of the ectodermal cells: $C1a$ seems pushed by the internal ectodermal flow of Fig. 2 (boxes $c3$-$c4$-$b4$); the motion of $C1b$, which is initially located near the external boundary might be initiated by the rounding of the initially asymmetric aggregates. In a recent work on phase separation in fluids, Nikolayev, Beysens, and Guenoun showed that the flow generated by the coalescence of two drops was able to generate coalescence with neighboring drops [28]. We cannot conclude that ectodermal flows generate endodermal cluster coalescence, but they may act on clusters like $C2a$. Thus separating intrinsic cluster motion (random deformation and displacements) from motion

caused by the surrounding mass of ectodermal cells is difficult.

Coherent motion. In all our experiments, even in the absence of rounding or sorting, we found short range spatial correlations corresponding to the parallel displacement of adjacent cells in Fig. 2. Thus cells move locally as coherent groups, even if the displacements of these groups are random over long time intervals (larger than the correlation time). The large collective rearrangement of the peripheral cells observed during sample 4 rounding [Fig. 5(c)] or during sorting in sample 2 (Fig. 3) is a macroscopic coherent motion. In sample 4, coherent motion is obviously caused by aggregate rounding. Coherent motion of endodermal cells is also observed during the rounding of endodermal clusters (see box $b4$ in Fig. 2) or the rounding of pure endodermal aggregates [27]. In sample 2, coherent motion is due to the internal sorting itself. Clusters progressively coalesce, round, and move to a central position in the aggregate. On average over long time scales, the ectodermal cells (and the nonaggregating endodermal cells) move toward the periphery of the aggregate, explaining the long time-scale correlations [Fig. 8(b)]. Ectodermal cells cannot escape from regions where clusters grow by diffusion. Indeed, the net displacement of single cells by random diffusion during one hour (10 μm, taking $D=1.5\ \mu m^2/min$) is often smaller than the displacements of clusters (12 μm on average over the clusters analyzed) or than the coherent displacements of endodermal cells inside clusters. As a result, ectodermal cells flow as liquids with velocities larger than 20 μm/min. When the endodermal density is high (e.g., 55% in sample 2), most of the ectodermal cells, which are confined in narrow channels, are affected by these flows. When the density is smaller as in sample 1 (40%), some flows are generated by the rounding of nearby clusters (e.g., boxes $c3$-$c4$-$b4$ in Fig. 2), but much of the ectoderm is not affected by flows.

Once a configuration with a rounded aggregate and rounded clusters is reached, coherent motion should stop. If several distant clusters are then present as in Fig. 1(c), final coalescence will take a very long time. In experiments using 100-μm spacers corresponding to aggregates with six layers of cells, we have always observed complete sorting [29]. Thus we believe that sorting is easier in three dimensions. For a given concentration, endodermal cells are closer together, and may easily percolate. Completion of cell sorting then occurs by the rounding of a single mass without requiring the displacement of distant clusters.

Origin of coherent motion. The macroscopic coherent motion observed in our experiments is driven by surface tension. However, liquidlike motion is not the only possible correlated cell motion. For example, in chicken embryo aggregates [9] and in simulations [13], the short time motion of nearby cells is uncorrelated even in the presence of long time correlations due to internal sorting [30].

This different behavior in chicken and hydra cell aggregates might result if the forces driving sorting and rounding (i.e., ectoderm-endoderm surface tension for internal sorting and external medium-ectoderm surface tension for aggregate rounding) are larger for hydra cells than for chicken embryo cells. This hypothesis, which should be easy to check experimentally [11], explains the faster completion of sorting in hydra aggregates. Higher surface tensions may be due to higher heterotypic surface energies, or to lower homotypic surface energies (larger homotypic adhesion) [31]. Higher heterotypic surface energies do not imply that ectodermal behavior is more or less liquidlike as chick cells diffuse less than hydra cells. They do not explain also why local coherent motion is observed, even in the absence of rounding or sorting. On the other hand, these observations can be accounted for from packing constraint considerations and from homotypic adhesion effects. Cells are nearly close packed in 2D aggregates. Thus, even by changing their shape, they cannot move independently of each other. Phillips and Steinberg suggested from an observation of the shape relaxation of centrifuged aggregates that coherent motion arises when cells are strongly but not irreversibly bound to one another [18]. Irreversible bonds prevent relative motion between cells. If homotypic pairs of hydra cells are more strongly bound to one another than pairs of chicken cells, they must move as coherent groups. Tight bonds, could account for both local and macroscopic coherent motion in our experiments. Simulations [13], lacking tight bonds, show an uncorrelated short time motion of nearby cells [30]. Correlated displacements of cells are observed in *dictyostelium* aggregation [19] and in *myxobacterium* aggregation [20]. They may also be due to tight bonds.

Conclusion. Combining *hydra viridissima* and 2D geometry allows us to visualize endodermal cell movements during cell sorting. The motion of cells and clusters consists of both random and coherent parts. Our results exclude any long range signaling between cells (chemotaxis). Our overall picture of sorting is the following: random fluctuations of single endodermal cells create small clusters by accretion; adjacent clusters are brought into contact by cluster deformations, and coalesce; cells move randomly until homotypic contact; then, coherent motion of endodermal cells driven by surface tension causes rounding of large clusters, and induces coherent motion in the ectodermal cells. We are currently varying the initial cell configuration to investigate the role of random cluster deformations and the conditions for coherent motion.

ACKNOWLEDGMENTS

One of the authors (J.P.R.) would like to thank J. Glazier for a critical reading of the manuscript. This work was supported by a Japanese Grant-in-Aid for Science Research Fund from the Ministry of Education, Science and Culture (No. 08409002, 40020400). J.P.R. acknowledges support from the Japan Society for the Promotion of Science (JSPS).

[1] P. Armstrong, Crit. Rev. Biochem. Mol. Biol. **24**, 119 (1989) (review article).

[2] A. Gierer, S. Berking, H. Bode, C. N. David, K. Flick, G. Hansmann, H. Schaller, and E. Trenkner, Nature New Biol. **239**, 98 (1972).

[3] H. R. Bode and P. M. Bode, Dev. Biol. **78**, 484 (1980).

[4] M. Sato and Y. Sawada, Dev. Biol. **133**, 119 (1989); M. Sato, H. Bode, and Y. Sawada, *ibid.* **141**, 412 (1990); M. Sato, H. Tashiro, A Oikawa, and Y. Sawada, *ibid.* **151**, 111 (1992); H. Shimizu, Y. Sawada, and T. Sugiyama, *ibid.* **155**, 287 (1993);

T. Itayama and Y. Sawada, J. Exp. Zool. **273**, 519 (1995).
[5] U. Technau and T. Holstein, Dev. Biol. **151**, 117 (1992).
[6] M. S. Steinberg, Proc. Natl. Acad. Sci. USA **48**, 1577 (1962); M. S. Steinberg, Science **137**, 762 (1962).
[7] J. P. Trinkaus and J. P. Lentz, Dev. Biol. **9**, 115 (1964).
[8] M. S. Steinberg, J. Exp. Zool. **173**, 395 (1970).
[9] J. C. Mombach, J. A. Glazier, R. C. Raphael, and M. Zajac, Phys. Rev. Lett. **75**, 2244 (1995).
[10] M. S. Steinberg, Proc. Natl. Acad. Sci. USA **48**, 1769 (1962); Science **141**, 401 (1963); J. Theor. Biol. **55**, 431 (1975).
[11] R. A. Foty, G. Forgacs, C. M. Pfleger, and M. S. Steinberg, Phys. Rev. Lett. **72**, 2298 (1994); R. A. Foty, C. M. Pfleger, G. Forgacs, and M. S. Steinberg, Development **122**, 1611 (1996).
[12] M. Sato-Maeda, M. Uchida, F. Graner, and H. Tashiro, Dev. Biol. **162**, 77 (1994).
[13] F. Graner and J. A. Glazier, Phys. Rev. Lett. **69**, 2013 (1992); J. A. Glazier and F. Graner, Phys. Rev. E **47**, 2128 (1993).
[14] E. Evans and K. Rithcie, Biophys. J. **72**, 1541 (1997).
[15] For a discussion of the reversibility of cell adhesion, see G. I. Bell, M. Dembo, and P. Bongrand, Biophys. J. **45**, 1051 (1984); *Physical Basis of Cell-Cell Adhesion*, edited by P. Bongrand (CRC, Boca Raton, 1988), Chaps. 7 and 10.
[16] J. C. Mombach and J. A. Glazier, Phys. Rev. Lett. **76**, 3032 (1996).
[17] P. Schaap, Differenciation **33**, 1 (1986); I. Takeuchi, T. Kakutani, and M. Tasaka, Dev. Genetics **9**, 607 (1988); K. W. Doolittle, I. Reddy, and J. G. McNally, Dev. Biol. **167**, 118 (1995); D. Traynor, R. H. Kessin, and J. G. Williams, Proc. Natl. Acad. Sci. USA **89**, 8303 (1992).
[18] H. M. Phillips and M. S. Steinberg, J. Cell. Sci. **30**, 1 (1978).
[19] W. F. Loomis, *The Development of Dictyostelium Discoideum* (Academic, New York, 1982).
[20] S. K. Kim and D. Kaiser, Science **249**, 926 (1990).
[21] R. D. Campbell, J. Cell. Sci. **13**, 651 (1973).
[22] Y. Kishimoto, M. Murate, and T. Sugiyama, J. Cell. Sci. **109**, 763 (1996).
[23] NIH Image is a public domain program developed at the U.S. National Institutes of Health and available on the Internet at http://rsb.info.nih.gov/nih-image/.
[24] M. Schindl, E. Wallraff, B. Deubzer, W. Witke, G. Gerish, and E. Sackmann, Biophys. J. **68**, 1177 (1995).
[25] M. S. Steinberg and D. R. Garrod, J. Cell. Sci. **18**, 385 (1975); D. R. Garrod and M. S. Steinberg, *ibid.* **18**, 405 (1975).
[26] D. Bray, *Cell Movements* (Garland, New York, 1992), Chap. 2.
[27] J. P. Rieu and Y. Sawada (unpublished).
[28] V. S. Nikolayev, D. Beysens, and P. Guenoun, Phys. Rev. Lett. **76**, 3144 (1996).
[29] T. Mizuguchi, Master's thesis, Tohoku University, 1995 (in Japanese).
[30] J. A. Glazier (private communication).
[31] For a clear definition of surface energies and surface tensions, see F. Graner, J. Theor. Biol. **164**, 455 (1993).